Fully charm and bottom pentaquarks in a lattice-QCD inspired quark model

Gang Yang,[1,*] Jialun Ping,[2,†] and Jorge Segovia[3,‡]

[1]*Department of Physics, Zhejiang Normal University, Jinhua 321004, China*
[2]*Department of Physics and Jiangsu Key Laboratory for Numerical Simulation of Large Scale Complex Systems, Nanjing Normal University, Nanjing 210023, China*
[3]*Departamento de Sistemas Físicos, Químicos y Naturales, Universidad Pablo de Olavide, E-41013 Sevilla, Spain*

(Received 26 May 2022; accepted 23 June 2022; published 6 July 2022)

The fully charm and bottom pentaquarks, i.e., $ccccc\bar{c}$ and $bbbbb\bar{b}$, with spin-parity quantum numbers $J^P = \frac{1}{2}^-$, $\frac{3}{2}^-$, and $\frac{5}{2}^-$, are investigated within a lattice-QCD inspired quark model, which has already successfully described the recently announced fully charm tetraquark candidate $X(6900)$ and has also predicted several other fully heavy tetraquarks. A powerful computational technique, based on the Gaussian expansion method combined with a complex-scaling range approach, is employed to predict, and distinguish, bound, resonance, and scattering states of the mentioned five-body system. Both baryon-meson and diquark-diquark-antiquark configurations, along with all of their possible color channels are comprehensively considered. Narrow resonances are obtained in each spin-parity channel for the fully charm and bottom systems. Moreover, most of them seem to be compact multiquarks whose wave functions are dominated by either hidden-color baryon-meson or diquark-diquark-antiquark structure or by the coupling between them.

DOI: 10.1103/PhysRevD.106.014005

I. INTRODUCTION

One century of fundamental research in atomic and nuclear physics has shown that all matter is corpuscular. The atoms that comprise us contain a dense nuclear core, which is composed of protons and neutrons, referred to collectively as nucleons, which are members of a broader class of femtometer-scale particles, called hadrons. In our understanding of hadrons, we have discovered that they are complicated bound states of quarks (and gluons) whose interactions are described by a quantum non-Abelian gauge field theory called quantum chromodynamics.

A very successful classification scheme for hadrons in terms of their valence quarks and antiquarks was independently proposed by Murray Gell-Mann [1] and George Zweig [2] in 1964. This classification (3-quarks) was called the quark model; it basically separates hadrons in two big families: mesons (quark-antiquark) and baryons (three-quarks). The quark model received experimental verification beginning in the late 1960s, and despite extensive experimental searches, no unambiguous candidates for exotic quark-gluon configurations were identified until 2003, when the Belle Collaboration discovered an unexpected enhancement at 3872 MeV in the $\pi^+\pi^- J/\psi$ invariant mass spectrum while studying the reaction $B^+ \to K^+\pi^+\pi^- J/\psi$ [3].

The so-called $X(3872)$ state challenged the quark model picture, leading to an explosion of related experimental activity since then. Consequently, more than 20 different charmonium- and bottomoniumlike XYZ states have been reported by worldwide experimental collaborations. Very detailed reviews have been published on the current state of the subject; see, for instance, Refs. [4–18]. In the last few years, more tetraquark candidates have been reported such as the charged charmoniumlike tetraquark with strangeness $X_{0,1}(2900)$ [19,20]; $X(2600)$ [21]; $X(1835)$, $X(2120)$, and $X(2370)$ [22]; $Z_{cs}(3985)$ [23]; $Z_{cs}(4000)$, $Z_{cs}(4220)$, $X(4630)$, and $X(4685)$ [24]; $Y(4230)$ and $Y(4500)$ [25]; the hidden charm structure $\psi_2(3823)$ [26,27]; and the doubly charmed tetraquark T_{cc}^+ [28,29]. In the baryon sector, experimental progress has been also developed; the first hidden-charm pentaquark $P_c^+(4380)$ was reported in 2015 by the LHCb Collaboration [30], and then more candidates were announced, e.g., the $P_c^+(4312)$, $P_c^+(4337)$, $P_c^+(4440)$, and $P_c^+(4457)$ [31,32] and also the hidden-charm pentaquark with strangeness $P_{cs}^0(4459)$ [33].

*yanggang@zjnu.edu.cn
†jlping@njnu.edu.cn
‡jsegovia@upo.es

In support of the experimental effort, theorists have been proposing different kinds of color-singlet clusters made by quarks, antiquarks, and gluons which go beyond conventional mesons and baryons. In fact, at the birth of the quark model, Gell-Mann and Zweig indicated already that hadronic states with $qq\bar{q}\,\bar{q}$ and $qqqq\bar{q}$ content should exist in nature. More concretely, recent studies on tetraquarks that include mass spectrum, structure, decay, and production properties can be found in, for instance, Refs. [34–44]. Besides, many analyses on hidden-charm pentaquarks P_c and P_{cs} have been published in the last few years [45–71]. Meanwhile, several other types of pentaquarks are theoretically studied, such as the hidden-strange and -bottom pentaquarks [72–75] as well as the single-charmed and doubly charmed pentaquarks [76–82].

The fully heavy tetraquark states $QQ\bar{Q}\,\bar{Q}$ $(Q = c,\ b)$ have recently attracted much attention. In 2017, the CMS Collaboration reported a benchmark measurement of $\Upsilon(1S)$-pair production in pp collisions at $\sqrt{s} = 8$ TeV [83] whose preliminary analysis seems to indicate an excess at 18.4 GeV in the $\Upsilon(1S)\ell^+\ell^-$ decay channel [84]. Besides, a significant peak at 18.2 GeV was observed in Cu + Au collisions at the Relativistic Heavy Ion Collider [85], but the LHCb and CMS collaborations [86,87] were not able to confirm it from the $\Upsilon(1S)\mu^+\mu^-$ invariant mass spectrum. Nevertheless, in the di-J/ψ invariant mass spectrum, a narrow peak at 6.9 GeV, a broad one between 6.2 and 6.8 GeV, and a hint for a possible structure around 7.2 GeV were reported by the LHCb Collaboration [88].

The identification of fully heavy tetraquark states make one speculate that the pentaquark system consisting of all heavy quarks, i.e., $QQQQ\bar{Q}$ with Q either a c or b quark, may also exist. The theoretical study of the masses and decay properties would help to search for the heavy pentaquark states in experiments. In fact, all investigations to date are as follows: the fully charm pentaquark state should have a mass at around 7.9 GeV according to quark models [89–91] and QCD sum rules [92,93], and it is claimed by the same works that the fully bottom pentaquark should be located at approximately 23 GeV.

In view of the complexity of the problem at hand, the only way toward progress is the use of a diverse array of theoretical approaches. In this work, we explore the possibility of having bound, resonance, and scattering states of fully charm and bottom pentaquarks, viz, $QQQQ\bar{Q}$ $(Q = c,\ b)$, with spin-parity $J^P = \frac{1}{2}^-$, $\frac{3}{2}^-$, and $\frac{5}{2}^-$ in the S-wave channel. We employ a nonrelativistic quark model with a two-body interaction between heavy quarks based on the lattice-QCD study of Ref. [94] and successfully applied by us to the case of fully heavy tetraquarks in Ref. [95]. The five-body problem is solved by using the Gaussian expansion method [96] combined with the complex scaling method [97–100] according to the so-called ABC theorem [97,98].

This work is organized in the following way. First, we briefly discuss the potential model, pentaquark wave functions, and computational method in Sec. II. Then, Sec. III is devoted to the analysis and discussion of our theoretical findings. A summary follows in Sec. IV.

II. THEORETICAL FRAMEWORK

The nature of heavy quarks, either charm or bottom, can be well described within a nonrelativistic quark model. Furthermore, inspired by lattice-regularized QCD investigations such as Ref. [94], the interplay between a heavy quark, Q, and a heavy antiquark, $\bar{Q}$, can be well approximated by the spin-independent Cornell potential along with a spin-spin interaction [101,102]. Accordingly, the Hamiltonian of the five heavy-quark system can be generally expressed as

$$H = \sum_{i=1}^{5}\left(M_Q + \frac{\vec{p}_i^{\,2}}{2M_Q}\right) + \sum_{j>i=1}^{5} V(\vec{r}_{ij}), \tag{1}$$

where M_Q is the mass of heavy quark (antiquark) and the two-body interacting potential can be written as

$$V(\vec{r}_{ij}) = -\frac{3}{16}(\lambda_i^a \cdot \lambda_j^a)\left[-\frac{\alpha}{r_{ij}} + \sigma r_{ij} + \beta e^{-\gamma r_{ij}}(\vec{s}_i \cdot \vec{s}_j)\right], \tag{2}$$

where, sorting by appearance, it includes Coulomb, linear confining, and spin-spin interactions. Moreover, color dependence is encoded in the SU(3) Gell-Mann matrices, λ_i^a $(a = 1, 2, \ldots, 8)$, and this factor is crucial in studying multiquark systems. Table I shows the model parameters: α, β, γ, and σ, determined by fitting the conventional $Q\bar{Q}$ meson spectrum [95,103], and the theoretical and experimental data are summarized in Table II. One can see that theoretical masses are consistent with their experimental counterparts. Although Ω_{ccc} and Ω_{bbb} baryons are still not seen by experiments, our calculated results are compatible with several other theoretical predictions [90,91,104]. Therefore, this fact provides a solid ground to further study possible bound and resonance states in the fully

TABLE I. Model parameters.

Quark masses	M_c (GeV)	1.290
	M_b (GeV)	4.700
Coulomb	α	0.4105
Confinement	σ(GeV^2)	0.2
Spin-spin	γ(GeV)	1.982
	β_{cc} (GeV)	2.06
	β_{bb} (GeV)	0.318

TABLE II. Theoretical and experimental masses, in MeV, for the S-wave conventional $Q\bar{Q}$ mesons and QQQ baryons.

State	M_{theory}	$M_{\text{experiment}}$
$\eta_c(1S)$	2968	2981
$\eta_c(2S)$	3655	3639
$\eta_c(3S)$	4152	…
$J/\psi(1S)$	3102	3097
$\psi(2S)$	3720	3686
$\psi(3S)$	4200	…
$\eta_b(1S)$	9401	9398
$\eta_b(2S)$	9961	9999
$\eta_b(3S)$	10316	…
$\Upsilon(1S)$	9463	9460
$\Upsilon(2S)$	9981	10023
$\Upsilon(3S)$	10330	10355
$\Omega_{ccc}(1S)$	4797	…
$\Omega_{ccc}(2S)$	5305	…
$\Omega_{ccc}(3S)$	5735	…
$\Omega_{bbb}(1S)$	14358	…
$\Omega_{bbb}(2S)$	14765	…
$\Omega_{bbb}(3S)$	15083	…

heavy pentaquark systems $QQQQ\bar{Q}$ and naturally continue our work done for fully heavy tetraquarks in Ref. [95].

In the present investigation, both baryon-meson and diquark-diquark-antiquark configurations, shown in Fig. 1, are simultaneously considered. Moreover, we comprehensively include all possible color structures compatible with the mentioned five-quark configurations and also allowed by the S-wave $J^P = 1/2^-$, $3/2^-$, and $5/2^-$ quantum numbers studied. Additionally, different kinds of coupled-channel calculations have been performed: the case in which a particular quark arrangement configuration is considered and the one where a complete coupled-channel computation is performed. Below, details on the fully heavy pentaquark wave functions along with our computational approach are illustrated.

A. Color, flavor, and spin structure

The pentaquark wave function is a product of four terms: color, flavor, spin, and space. Concerning the color degree of freedom, there is a richer color structure in multiquark systems than in conventional quark-antiquark and three-quark hadrons. Particularly, the colorless wave function of a five-body system can be obtained through either a color-singlet or a hidden-color channel or both. Since baryon-meson and diquark-diquark-antiquark configurations are simultaneously considered in this investigation, the color-singlet channel can be reached considering only Fig. 1(a), whereas the hidden-color channel can be obtained through either Figs. 1(a) or 1(b). Note herein that, although it is enough to just consider the color singlet channel when all possible excited states of a system are included, a more efficient way of performing the computation is considering both the color singlet and hidden-color wave functions. The color-singlet wave function reads as

$$\chi_1^c = \frac{1}{\sqrt{18}}(rgb - rbg + gbr - grb + brg - bgr) \times (\bar{r}r + \bar{g}g + \bar{b}b), \tag{3}$$

and the hidden-color one corresponding to Fig. 1(a) is

$$\chi_k^c = \frac{1}{\sqrt{8}}(\chi_{3,1}^k\chi_{2,8} - \chi_{3,2}^k\chi_{2,7} - \chi_{3,3}^k\chi_{2,6} + \chi_{3,4}^k\chi_{2,5} + \chi_{3,5}^k\chi_{2,4} - \chi_{3,6}^k\chi_{2,3} - \chi_{3,7}^k\chi_{2,2} + \chi_{3,8}^k\chi_{2,1}), \tag{4}$$

where $k = 2(3)$ is an index which stands for the symmetric (antisymmetric) configuration of two quarks in the three-quark subcluster. In Eq. (4), all color bases of the two sub-clusters, meson and baryon, are those used in studying the P_c hidden-charm [71], P_b hidden-bottom [75], and doubly charmed pentaquarks [82]. Additionally, two colorless wave functions of the diquark-diquark-antiquark configuration of Fig. 1(b) are obtained. Considering the chains of color-coupling coefficients

(i) $[C^{[2]}_{[1],[1]}C^{[11]}_{[1],[1]}C^{[211]}_{[2],[11]}C^{[222]}_{[11],[211]}]_4$,

(ii) $[C^{[11]}_{[1],[1]}C^{[11]}_{[1],[1]}C^{[211]}_{[11],[11]}C^{[222]}_{[11],[211]}]_5$,

the two colorless wave functions of diquark-diquark-antiquark configuration are (subscripts correspond to the ones above):

$$\chi_4^c = \frac{1}{\sqrt{48}}\{\bar{r}[(rb+br)(rg-gr) - (rg+gr)(rb-br)] + \bar{g}[(rg+gr)(gb-bg) + (gb+bg)(rg-gr)] + \bar{b}[(rb+br)(gb-bg) - (gb+bg)(rb-br)] + \sqrt{2}[\bar{r}rr(gb-bg) - \bar{g}gg(rb-br) + \bar{b}bb(rg-gr)]\}, \tag{5}$$

$$\chi_5^c = \frac{1}{\sqrt{24}}\{\bar{r}[(rg-gr)(rb-br) - (rb-br)(rg-gr)] + \bar{g}[(rg-gr)(gb-bg) - (gb-bg)(rg-gr)] + \bar{b}[(rb-br)(gb-bg) - (gb-bg)(rb-br)]\}. \tag{6}$$

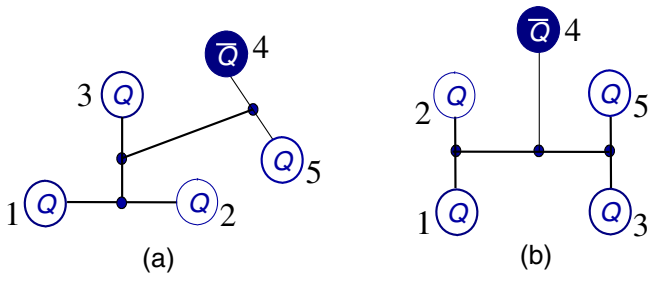

FIG. 1. Configurations in the fully heavy pentaquarks. Panel (a) is the baryon-meson structure, and panel (b) is the diquark-diquark-antiquark one ($Q = c$, b).

With respect the flavor wave function of fully charm and bottom pentaquarks, it is simply expressed as $\chi_I^f = QQQ\bar{Q}Q$ ($Q = c,\ b$), which corresponds to the quark sequence shown in Fig. 1 and simply gives a total isospin, I, equal to zero.

Only S-wave fully heavy pentaquark states shall be considered, and thus the total angular momentum, J, coincides with the spin, S, of the five-quark system which ranges from $1/2$ to $5/2$. Therefore, we should only focus on the possible spin wave functions of a fully heavy pentaquark system; the spin wave function of the baryon-meson structure of Fig. 1(a) can be written as (the third component of spin is taken to be equal to S without loss of generality)

$$\chi^{\sigma 1}_{\frac{1}{2},\frac{1}{2}}(5) = \sqrt{\frac{1}{6}}\chi^{\sigma}_{\frac{3}{2},-\frac{1}{2}}(3)\chi^{\sigma}_{11} - \sqrt{\frac{1}{3}}\chi^{\sigma}_{\frac{3}{2},\frac{1}{2}}(3)\chi^{\sigma}_{10} + \sqrt{\frac{1}{2}}\chi^{\sigma}_{\frac{3}{2},\frac{3}{2}}(3)\chi^{\sigma}_{1-1} \tag{7}$$

$$\chi^{\sigma 2}_{\frac{1}{2},\frac{1}{2}}(5) = \sqrt{\frac{1}{3}}\chi^{\sigma+}_{\frac{1}{2},\frac{1}{2}}(3)\chi^{\sigma}_{10} - \sqrt{\frac{2}{3}}\chi^{\sigma+}_{\frac{1}{2},-\frac{1}{2}}(3)\chi^{\sigma}_{11} \tag{8}$$

$$\chi^{\sigma 3}_{\frac{1}{2},\frac{1}{2}}(5) = \sqrt{\frac{1}{3}}\chi^{\sigma-}_{\frac{1}{2},\frac{1}{2}}(3)\chi^{\sigma}_{10} - \sqrt{\frac{2}{3}}\chi^{\sigma-}_{\frac{1}{2},-\frac{1}{2}}(3)\chi^{\sigma}_{11} \tag{9}$$

$$\chi^{\sigma 4}_{\frac{1}{2},\frac{1}{2}}(5) = \chi^{\sigma+}_{\frac{1}{2},\frac{1}{2}}(3)\chi^{\sigma}_{00} \tag{10}$$

$$\chi^{\sigma 5}_{\frac{1}{2},\frac{1}{2}}(5) = \chi^{\sigma-}_{\frac{1}{2},\frac{1}{2}}(3)\chi^{\sigma}_{00} \tag{11}$$

for $S = 1/2$ and

$$\chi^{\sigma 1}_{\frac{3}{2},\frac{3}{2}}(5) = \sqrt{\frac{3}{5}}\chi^{\sigma}_{\frac{3}{2},\frac{3}{2}}(3)\chi^{\sigma}_{10} - \sqrt{\frac{2}{5}}\chi^{\sigma}_{\frac{3}{2},\frac{1}{2}}(3)\chi^{\sigma}_{11} \tag{12}$$

$$\chi^{\sigma 2}_{\frac{3}{2},\frac{3}{2}}(5) = \chi^{\sigma}_{\frac{3}{2},\frac{3}{2}}(3)\chi^{\sigma}_{00} \tag{13}$$

$$\chi^{\sigma 3}_{\frac{3}{2},\frac{3}{2}}(5) = \chi^{\sigma+}_{\frac{1}{2},\frac{1}{2}}(3)\chi^{\sigma}_{11} \tag{14}$$

$$\chi^{\sigma 4}_{\frac{3}{2},\frac{3}{2}}(5) = \chi^{\sigma-}_{\frac{1}{2},\frac{1}{2}}(3)\chi^{\sigma}_{11} \tag{15}$$

for $S = 3/2$ and

$$\chi^{\sigma 1}_{\frac{5}{2},\frac{5}{2}}(5) = \chi^{\sigma}_{\frac{3}{2},\frac{3}{2}}(3)\chi^{\sigma}_{11} \tag{16}$$

for $S = 5/2$.

The possible spin wave functions for the diquark-diquark-antiquark configuration of Fig. 1(b), compatible with the quantum numbers that we are investigating, can be summarized as

$$\chi^{\sigma 6}_{\frac{1}{2},\frac{1}{2}}(5) = \chi^{\sigma}_{00}\chi^{\sigma}_{00}\chi^{\sigma}_{\frac{1}{2},\frac{1}{2}} \tag{17}$$

$$\chi^{\sigma 7}_{\frac{1}{2},\frac{1}{2}}(5) = \sqrt{\frac{2}{3}}\chi^{\sigma}_{00}\chi^{\sigma}_{11}\chi^{\sigma}_{\frac{1}{2},-\frac{1}{2}} - \sqrt{\frac{1}{3}}\chi^{\sigma}_{00}\chi^{\sigma}_{10}\chi^{\sigma}_{\frac{1}{2},\frac{1}{2}} \tag{18}$$

$$\chi^{\sigma 8}_{\frac{1}{2},\frac{1}{2}}(5) = \sqrt{\frac{1}{3}}(\chi^{\sigma}_{11}\chi^{\sigma}_{1-1} - \chi^{\sigma}_{10}\chi^{\sigma}_{10} + \chi^{\sigma}_{1-1}\chi^{\sigma}_{11})\chi^{\sigma}_{\frac{1}{2},\frac{1}{2}} \tag{19}$$

$$\chi^{\sigma 9}_{\frac{1}{2},\frac{1}{2}}(5) = \sqrt{\frac{1}{3}}(\chi^{\sigma}_{11}\chi^{\sigma}_{10} - \chi^{\sigma}_{10}\chi^{\sigma}_{11})\chi^{\sigma}_{\frac{1}{2},-\frac{1}{2}} - \sqrt{\frac{1}{6}}(\chi^{\sigma}_{11}\chi^{\sigma}_{1-1} - \chi^{\sigma}_{1-1}\chi^{\sigma}_{11})\chi^{\sigma}_{\frac{1}{2},\frac{1}{2}} \tag{20}$$

for $S = 1/2$ and

$$\chi^{\sigma 5}_{\frac{3}{2},\frac{3}{2}}(5) = \chi^{\sigma}_{00}\chi^{\sigma}_{11}\chi^{\sigma}_{\frac{1}{2},\frac{1}{2}} \tag{21}$$

$$\chi^{\sigma 6}_{\frac{3}{2},\frac{3}{2}}(5) = \sqrt{\frac{1}{2}}(\chi^{\sigma}_{11}\chi^{\sigma}_{10} - \chi^{\sigma}_{10}\chi^{\sigma}_{11})\chi^{\sigma}_{\frac{1}{2},\frac{1}{2}} \tag{22}$$

$$\chi^{\sigma 7}_{\frac{3}{2},\frac{3}{2}}(5) = \sqrt{\frac{4}{5}}\chi^{\sigma}_{11}\chi^{\sigma}_{11}\chi^{\sigma}_{\frac{1}{2},-\frac{1}{2}} - \sqrt{\frac{1}{10}}(\chi^{\sigma}_{11}\chi^{\sigma}_{10} + \chi^{\sigma}_{10}\chi^{\sigma}_{11})\chi^{\sigma}_{\frac{1}{2},\frac{1}{2}} \tag{23}$$

for $S = 3/2$ and

$$\chi^{\sigma 2}_{\frac{5}{2},\frac{5}{2}}(5) = \chi^{\sigma}_{11}\chi^{\sigma}_{11}\chi^{\sigma}_{\frac{1}{2},\frac{1}{2}} \tag{24}$$

for $S = 5/2$.

Note herein that all these expressions can be easily derived by considering the three-quark and quark-quark(antiquark) subclusters and using SU(2) algebra. Particularly, the spin bases which ranges from Eqs. (7)–(24), have been already derived by us when investigating other multiquark systems; further details can be found in Refs. [71,75,82].

B. Computational method

We have already mentioned that two sets of fully heavy pentaquark configurations, shown in Fig. 1, are considered. Consequently, their antisymmetry operators must be categorized. The antisymmetry operator for the baryon-meson structure of Fig. 1(a) is

$$\mathcal{A}_1 = [1 - (15) - (25) - (35)][1 - (13) - (23)]. \tag{25}$$

Meanwhile, the diquark-diquark-antiquark arrangement of Fig. 1(b) has an antisymmetry operator

$$\mathcal{A}_2 = 1 - (13) - (15) - (23) - (25) + (13)(25). \tag{26}$$

The Rayleigh-Ritz variational principle is employed herein to solve the Schrödinger-like five-body bound-state equation because it is one of the most extended tools to solve eigenvalue problems due to its simplicity and flexibility. Given a set of relative motion coordinates, where the center-of-mass kinetic term T_{CM} can be completely eliminated for a nonrelativistic system, the five-quark system spatial wave function is generally written as

$$\psi_{LM_L}(\theta) = [[[\phi_{n_1 l_1}(\vec{\rho}e^{i\theta})\phi_{n_2 l_2}(\vec{\lambda}e^{i\theta})]_l \phi_{n_3 l_3}(\vec{r}e^{i\theta})]_{l'} \phi_{n_4 l_4}(\vec{R}e^{i\theta})]_{LM_L}. \quad (27)$$

In particular, the four internal Jacobi coordinates of baryon-meson structure of Fig. 1(a) are defined in the following way:

$$\vec{\rho} = \vec{x}_1 - \vec{x}_2, \quad (28)$$

$$\vec{\lambda} = \vec{x}_3 - \frac{m_1\vec{x}_1 + m_2\vec{x}_2}{m_1 + m_2}, \quad (29)$$

$$\vec{r} = \vec{x}_4 - \vec{x}_5, \quad (30)$$

$$\vec{R} = \frac{m_1\vec{x}_1 + m_2\vec{x}_2 + m_3\vec{x}_3}{m_1 + m_2 + m_3} - \frac{m_4\vec{x}_4 + m_5\vec{x}_5}{m_4 + m_5}. \quad (31)$$

And, in the case of diquark-diquark-antiquark configuration of Fig. 1(b), they read as

$$\vec{\rho} = \vec{x}_1 - \vec{x}_2, \quad (32)$$

$$\vec{\lambda} = \vec{x}_3 - \vec{x}_5, \quad (33)$$

$$\vec{r} = \frac{m_1\vec{x}_1 + m_2\vec{x}_2}{m_1 + m_2} - \frac{m_3\vec{x}_3 + m_5\vec{x}_5}{m_3 + m_5}, \quad (34)$$

$$\vec{R} = \vec{x}_4 - \frac{m_1\vec{x}_1 + m_2\vec{x}_2 + m_3\vec{x}_3 + m_5\vec{x}_5}{m_1 + m_2 + m_3 + m_5}. \quad (35)$$

A crucial point of the Rayleigh-Ritz variational method is the basis expansion of the genuine state's wave function. Herein, the Gaussian expansion method (GEM) [96] is employed; each relative coordinate is expanded in terms of a Gaussian basis whose sizes are taken in geometric progression. Moreover, as mentioned above, GEM is complemented with the complex scaling method in order to have access at the same time to bound, resonance, and scattering states. This approach has been proven before to be quite efficient on solving the bound- and resonance-state problem of multiquark systems [71,75,82,95,105–107]. The interested reader is referred to Ref. [14] for a comprehensive summary on the GEM and complex scaling method (CSM) applied to multiquark systems. Consequently, the functional form of the orbital wave functions, ϕ, shown in Eq. (27) is

$$\phi_{nlm}(\vec{r}e^{i\theta}) = N_{nl}(re^{i\theta})^l e^{-\nu_n(re^{i\theta})^2} Y_{lm}(\hat{r}). \quad (36)$$

Only S-wave states of fully heavy pentaquarks are investigated in this work, and thus no laborious Racah algebra is needed when computing matrix elements. In other words, the value of the spherical harmonic function Y_{lm} is just a constant, viz., $Y_{00} = \sqrt{1/4\pi}$.

Finally, in order to fulfill the Pauli principle, the complete antisymmetric complex wave-function of five-quark system is written as

$$\Psi_{JM,i,j}(\theta) = \sum_{n=1}^{2} \mathcal{A}_n[[\psi_L(\theta)\chi_S^{\sigma_i}(5)]_{JM}\chi_I^f\chi_j^c], \quad (37)$$

where $\mathcal{A}_n$ is the antisymmetry operator whose expression is either Eq. (25) or Eq. (26) depending if baryon-meson or diquark-diquark-antiquark is accordingly considered. The use of these antisymmetric operators is needed because we have constructed an antisymmetric wave function for only two quarks of the three-quark subcluster in baryon-meson configuration or for the quark-quark subcluster in the diquark-diquark-antiquark arrangement; the remaining quarks in the system are coupled to the wave function by simply considering appropriate Clebsch-Gordan coefficients.

III. RESULTS

The S-wave low-lying states of fully charm and bottom pentaquarks are systematically investigated by taking into account both baryon-meson and diquark-diquark-antiquark configurations. Besides, all possible color structures of each configuration, along with their couplings, are comprehensively considered. The total angular momentum J, which coincides with the total spin S, ranges from $1/2$ to $5/2$ with a negative parity $P = -1$.

First, real-range investigations are performed on the fully heavy pentaquarks, and Tables III–XIV list our calculated results. In particular, masses of each channel in baryon-meson configuration and diquark-diquark-antiquark one, along with their couplings, are summarized in Tables III, V, and VII for the fully charm pentaquarks with $J^P = \frac{1}{2}^-$, $\frac{3}{2}^-$, and $\frac{5}{2}^-$, respectively. Besides, similar studies for the fully bottom pentaquarks are shown in Tables IX, XI, and XIII, respectively. Therein, the two considered configurations of pentaquark system, baryon-meson, and diquark-diquark-antiquark are listed in the first column. They are then assigned an index in the following column. The third one presents a particular combination of spin ($\chi_J^{\sigma_i}$) and color (χ_j^c) wave functions, compatible with the spin-parity quantum numbers considered in each case. The theoretical mass of each channel is shown in the fourth column, and the coupled result for each kind of configuration is presented in the last one. The last row of all those tables indicates the lowest-lying-coupled mass in a complete coupled-channel computation.

In a further step, the CSM is employed only for complete coupled-channel calculations of the $QQQQ\bar{Q}$ systems. Figures 2–7 show general distributions of the found complex eigenenergies; possible resonance states are indicated inside (orange) circles. Meanwhile, Tables IV, VI, and VIII are about compositeness of the obtained fully charm resonances within $\frac{1}{2}^-$, $\frac{3}{2}^-$, and $\frac{5}{2}^-$, respectively.

TABLE III. Lowest-lying fully charm pentaquark states with $J^P = 1/2^-$ calculated within a real range formulation of the potential quark model. Baryon-meson and diquark-diquark-antiquark configurations are listed in the first column, and the superscripts 1 and 8 stand for the color-singlet and -octet states, respectively. Each channel is assigned an index in the second column; it reflects a particular combination of spin ($\chi_J^{\sigma_i}$) and color (χ_j^c) wave functions that are shown explicitly in the third column. The theoretical mass obtained in each channel is shown in the fourth column, and the coupled result for each kind of configuration is presented in the last column. When a complete coupled-channel calculation is performed, last row of the table indicates the lowest-lying mass. (unit: MeV).

Channel	Index	$\chi_J^{\sigma_i};\chi_j^c$ $[i;j]$	M	Mixed
$(\Omega_{ccc}J/\psi)^1$	1	[1; 1]	7899	7899
$(\Omega_{ccc}J/\psi)^8$	2	[5; 2]	8088	
$(\Omega_{ccc}J/\psi)^8$	3	[4; 3]	8082	
$(\Omega_{ccc}J/\psi)^8$	4	[3; 2]	8145	
$(\Omega_{ccc}J/\psi)^8$	5	[2; 3]	8144	
$(\Omega_{ccc}J/\psi)^8$	6	[1; 3]	8556	8022
$(cc)(cc)^*\bar{c}$	7	[7; 4]	8142	
$(cc)^*(cc)^*\bar{c}$	8	[9; 5]	8098	
$(cc)^*(cc)^*\bar{c}$	9	[8; 5]	8167	8045
Complete coupled channel:				7899

TABLE IV. Compositeness of the exotic resonances for the $J^P = 1/2^-$ fully charm pentaquarks, obtained when a complete coupled-channel analysis using CSM is performed. Particularly, the first column is the resonance pole labeled by the $M + i\Gamma$, unit in MeV; the second one is the distance between any two quarks or quark-antiquark, unit in fm, and the last column is the component of each resonance state (S: baryon-meson structure in the color-singlet channel; H: baryon-meson structure in the hidden-color channel; Di: diquark-diquark-antiquark configuration).

Resonance	$(r_{cc}, r_{c\bar{c}})$	Component
$8098 + i0.16$	(0.53, 0.56)	Di: 100%
$8634 + i0.38$	(0.75, 0.64)	Di: 100%
$8742 + i0.86$	(0.76, 0.71)	S: 46%; H: 52.7%; Di: 1.3%

The resonance pole, encoded by its mass and width $(M + i\Gamma)$, is listed in the first column; its inner structure elucidated by quark-quark and quark-antiquark distances is shown in the second column; and the last column presents the dominant component of each resonance. The corresponding analyses for fully bottom pentaquarks are collected in Tables X, XII, and XIV, respectively.

We proceed now to describe in detail our theoretical findings.

TABLE V. Lowest-lying fully charm pentaquark states with $J^P = 3/2^-$ calculated within a real range formulation of the potential quark model. The results are similarly organized as those in Table III. (unit: MeV).

Channel	Index	$\chi_J^{\sigma_i};\chi_j^c$ $[i;j]$	M	Mixed
$(\Omega_{ccc}\eta_c)^1$	1	[2; 1]	7765	
$(\Omega_{ccc}J/\psi)^1$	2	[1; 1]	7899	7765
$(\Omega_{ccc}J/\psi)^8$	3	[4; 2]	7992	
$(\Omega_{ccc}J/\psi)^8$	4	[3; 3]	7987	
$(\Omega_{ccc}\eta_c)^8$	5	[2; 3]	8155	
$(\Omega_{ccc}J/\psi)^8$	6	[1; 3]	8259	7982
$(cc)(cc)^*\bar{c}$	7	[5; 4]	8104	
$(cc)^*(cc)^*\bar{c}$	8	[6; 5]	8131	
$(cc)^*(cc)^*\bar{c}$	9	[7; 5]	8095	8095
Complete coupled channel:				7765

TABLE VI. Compositeness of the exotic resonances for the $J^P = 3/2^-$ fully charm pentaquarks, obtained when a complete coupled-channel analysis using CSM is performed. The results are similarly organized as those in Table IV.

Resonance	$(r_{cc}, r_{c\bar{c}})$	Component
$8095 + i0.14$	(0.53, 0.55)	Di: 100%
$8656 + i0.62$	(0.76, 0.65)	Di: 100%

TABLE VII. Lowest-lying fully charm pentaquark states with $J^P = 5/2^-$ calculated within a real range formulation of the potential quark model. The results are similarly organized as those in Table III. (unit: MeV).

Channel	Index	$\chi_J^{\sigma_i};\chi_j^c$ $[i;j]$	M	Mixed
$(\Omega_{ccc}J/\psi)^1$	1	[1; 1]	7899	7899
$(\Omega_{ccc}J/\psi)^8$	2	[1; 3]	8421	8421
$(cc)^*(cc)^*\bar{c}$	3	[1; 5]	8137	8137
Complete coupled channel:				7899

TABLE VIII. Compositeness of the exotic resonances for the $J^P = 5/2^-$ fully charm pentaquarks, obtained when a complete coupled-channel analysis using CSM is performed. The results are similarly organized as those in Table IV.

Resonance	$(r_{cc}, r_{c\bar{c}})$	Component
$8137 + i0.18$	(0.53, 0.57)	Di: 100%
$8668 + i0.62$	(0.74, 0.68)	Di: 100%
$8727 + i0.64$	(0.75, 0.65)	S: 11.1%; H: 37.9%; Di: 51%

TABLE IX. Lowest-lying fully bottom pentaquark states with $J^P = 1/2^-$ calculated within a real range formulation of the potential quark model. The results are similarly organized as those in Table III. (unit: MeV).

Channel	Index	$\chi_J^{\sigma_i};\chi_j^c$ $[i;j]$	M	Mixed
$(\Omega_{bbb}\Upsilon)^1$	1	[1; 1]	23821	23821
$(\Omega_{bbb}\Upsilon)^8$	2	[5; 2]	24028	
$(\Omega_{bbb}\Upsilon)^8$	3	[4; 3]	24016	
$(\Omega_{bbb}\Upsilon)^8$	4	[3; 2]	24032	
$(\Omega_{bbb}\Upsilon)^8$	5	[2; 3]	24075	
$(\Omega_{bbb}\Upsilon)^8$	6	[1; 3]	24443	23959
$(bb)(bb)^*\bar{b}$	7	[7; 4]	24066	
$(bb)^*(bb)^*\bar{b}$	8	[9; 5]	24055	
$(bb)^*(bb)^*\bar{b}$	9	[8; 5]	24093	24035
Complete coupled channel:				23821

TABLE X. Compositeness of the exotic resonances for the $J^P = 1/2^-$ fully bottom pentaquarks, obtained when a complete coupled-channel analysis using CSM is performed. The results are similarly organized as those in Table IV.

Resonance	$(r_{bb}, r_{b\bar{b}})$	Component
$24026 + i0.06$	(0.29, 0.30)	S: 4.6%; H: 36.5%; Di: 58.9%
$24055 + i0.12$	(0.29, 0.31)	Di: 100%
$24591 + i0.08$	(0.44, 0.42)	S: 46.2%; H: 52.3%; Di: 1.5%

TABLE XI. Lowest-lying fully bottom pentaquark states with $J^P = 3/2^-$ calculated within a real range formulation of the potential quark model. The results are similarly organized as those in Table III. (unit: MeV).

Channel	Index	$\chi_J^{\sigma_i};\chi_j^c$ $[i;j]$	M	Mixed
$(\Omega_{bbb}\eta_b)^1$	1	[2; 1]	23759	
$(\Omega_{bbb}\Upsilon)^1$	2	[1; 1]	23821	23759
$(\Omega_{bbb}\Upsilon)^8$	3	[4; 2]	23955	
$(\Omega_{bbb}\Upsilon)^8$	4	[3; 3]	23942	
$(\Omega_{bbb}\eta_b)^8$	5	[2; 3]	24347	
$(\Omega_{bbb}\Upsilon)^8$	6	[1; 3]	24374	23936
$(bb)(bb)^*\bar{b}$	7	[5; 4]	24045	
$(bb)^*(bb)^*\bar{b}$	8	[6; 5]	24074	
$(bb)^*(bb)^*\bar{b}$	9	[7; 5]	24054	24035
Complete coupled channel:				23759

TABLE XII. Compositeness of the exotic resonances for the $J^P = 3/2^-$ fully bottom pentaquarks, obtained when a complete coupled-channel analysis using CSM is performed. The results are similarly organized as those in Table IV.

Resonance	$(r_{bb}, r_{b\bar{b}})$	Component
$24059 + i0.02$	(0.30, 0.31)	S: 4.5%; H: 39.3%; Di: 56.2%
$24468 + i0.22$	(0.34, 0.49)	Di: 100%

TABLE XIII. Lowest-lying fully bottom pentaquark states with $J^P = 5/2^-$ calculated within a real range formulation of the potential quark model. The results are similarly organized as those in Table III. (unit: MeV).

Channel	Index	$\chi_J^{\sigma_i};\chi_j^c$ $[i;j]$	M	Mixed
$(\Omega_{bbb}\Upsilon)^1$	1	[1; 1]	23821	23821
$(\Omega_{bbb}\Upsilon)^8$	2	[1; 3]	24302	24302
$(bb)^*(bb)^*\bar{b}$	3	[1; 5]	24076	24076
Complete coupled channel:				23821

TABLE XIV. Compositeness of the exotic resonances for the $J^P = 5/2^-$ fully bottom pentaquarks, obtained when a complete coupled-channel analysis using CSM is performed. The results are similarly organized as those in Table IV.

Resonance	$(r_{bb}, r_{b\bar{b}})$	Component
$24076 + i0.12$	(0.29, 0.31)	Di: 100%
$24478 + i0.46$	(0.32, 0.49)	Di: 100%

A. Fully charm pentaquarks

1. $J^P = \frac{1}{2}^-$ sector

Table III shows our results in this case. There is only one color-singlet baryon-meson channel, $\Omega_{ccc}J/\psi$. Its calculated lowest mass is just the noninteracting baryon-meson threshold value 7899 MeV. Meanwhile, the five hidden-color configurations of $\Omega_{ccc}J/\psi$ are above 8.0 GeV, ranging from 8.08 to 8.56 GeV. Three hidden-color diquark-diquark-antiquark channels are around 8.1 GeV. When performing a coupled-channel calculation in each exotic configuration: hidden-color baryon-meson and diquark-diquark-antiquark, the lowest masses are 8.02 and 8.04 GeV, respectively. Therefore, no bound state is found, and this fact remains unchanged within a complete coupled-channel real-range calculation.

In a further step where the complex scaling method is employed in a fully coupled-channel calculation, the scattering states of $\Omega_{ccc}(1S)J/\psi(1S)$, $\Omega_{ccc}(2S)J/\psi(1S)$,

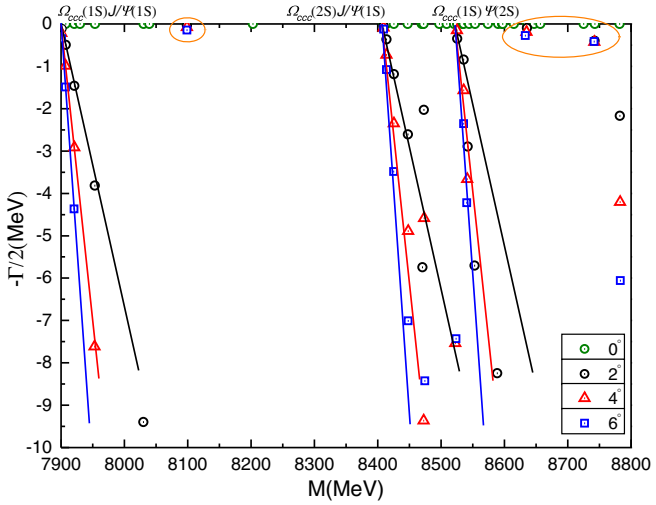

FIG. 2. Complex eigenenergies of coupled-channel calculation for various θ within $J^P = \frac{1}{2}^-$.

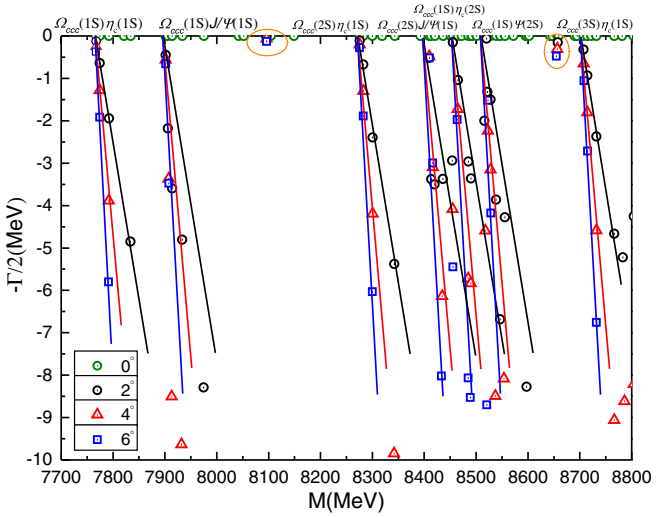

FIG. 3. Complex eigenenergies of coupled-channel calculation for various θ within $J^P = \frac{3}{2}^-$.

and $\Omega_{ccc}(1S)J/\psi(2S)$ are shown well in Fig. 2 within an energy gap 7.9–8.8 GeV. Therein, with a rotated angle varied from 0° to 6°, the vast majority of complex energies is aligned well on their corresponding threshold lines. However, three fixed poles, which are independent of θ, are clearly obtained. They are quite narrow resonances, and the complex energies, denoted as $M + i\Gamma$, are $(8098 + i0.16)$ MeV, $(8634 + i0.38)$ MeV, and $(8742 + i0.86)$ MeV, respectively.

We compute the quark–(anti)quark distances and the dominant wave function component in our analysis about the compositeness of these three resonance poles. Table IV shows our results; one can conclude that these five-quark exotic resonances are compact with a size around 0.5–0.8 fm. This nature is also confirmed by their dominant component which is either diquark-diquark-antiquark or hidden-color baryon-meson. It is worth noting that our result on the first resonance at $(8098 + i0.16)$ MeV is also supported by Ref. [92], whose calculated mass upper limit for the fully charm pentaquark of diquark-diquark-antiquark nature and $J^P = \frac{1}{2}^-$ quantum numbers is 8.08 GeV.

2. $J^P = \frac{3}{2}^-$ sector

Table V shows that there are also nine channels to be considered in this fully charm pentaquark sector. In particular, there are two color-singlet baryon-meson structures, $\Omega_{ccc}\eta_c$ and $\Omega_{ccc}J/\psi$; four hidden-color channels of the same baryon-meson nature; and three diquark-diquark-antiquark cases. First of all, when a calculation in each single channel is performed, the lowest mass 7765 MeV is just the theoretical threshold value of $\Omega_{ccc}\eta_c$; moreover, there is another calculated color-singlet mass with a value of 7899 MeV which is located at the $\Omega_{ccc}J/\psi$ threshold, and the other exotic channels are generally lying within an interval of 7.99–8.26 GeV. When a coupled-channel computation is performed in each particular pentaquark configuration, the masses are all located above $\Omega_{ccc}\eta_c$ threshold, and they are 7765, 7982, and 8095 MeV for the color-singlet baryon-meson, hidden-color baryon-meson, and diquark-diquark-antiquark cases, respectively. The last row of Table V shows the lowest computed mass, 7765 MeV, when a complete coupled-channel computation in real range formalism is performed; therefore, no bound states are found for fully charm pentaquarks with $J^P = 3/2^-$ quantum numbers.

Figure 3 presents the distribution of complex eigenenergies of the $J^P = 3/2^-$ fully charm pentaquark system when a complete coupled-channel analysis is carried out using the CSM. Within the energy interval 7.7–8.8 GeV, the ground states of $\Omega_{ccc}\eta_c$ and $\Omega_{ccc}J/\psi$, along with their radial excitations, are well presented. These baryon-meson states are of scattering nature, with calculated discrete energies always going down with respect to the variation of complex angle θ. Nevertheless, two extremely narrow resonances survive among these continuum states.

The theoretical poles are located at $(8095 + i0.14)$ and $(8656 + i0.62)$ MeV. Hence, it seems that the lowest resonances of fully charm pentaquarks with $\frac{1}{2}^-$ and $\frac{3}{2}^-$ quantum numbers are degenerate. Additionally, Table VI analyzes the compositeness of the two poles found in this channel, and one may conclude that they are quite compact whose sizes are less than 0.8 fm and their dominant wave function's components are of diquark-diquark-antiquark type.

3. $J^P = \frac{5}{2}^-$ sector

In the highest spin case of fully charm pentaquarks, there are only three possible configurations under consideration, i.e., just one state of singlet-color baryon-meson, hidden-color baryon-meson, and diquark-diquark-antiquark. The calculated mass results are listed in Table VII; it is worth highlighting that the unbound nature of the $\Omega_{ccc}J/\psi$,

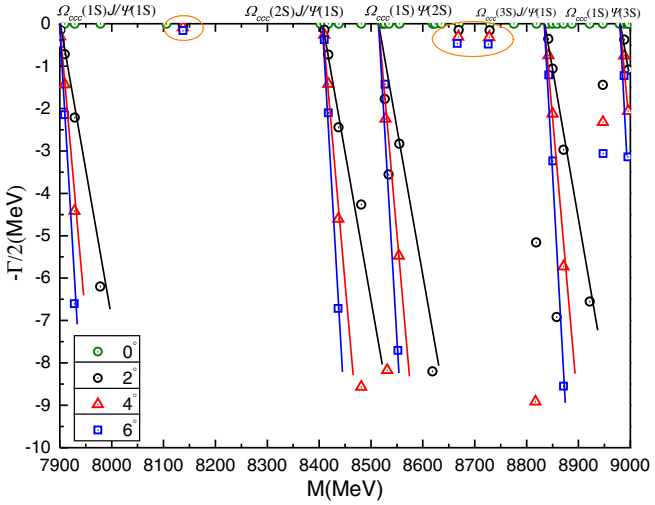

FIG. 4. Complex eigenenergies of coupled-channel calculation for various θ within $J^P = \frac{5}{2}^-$.

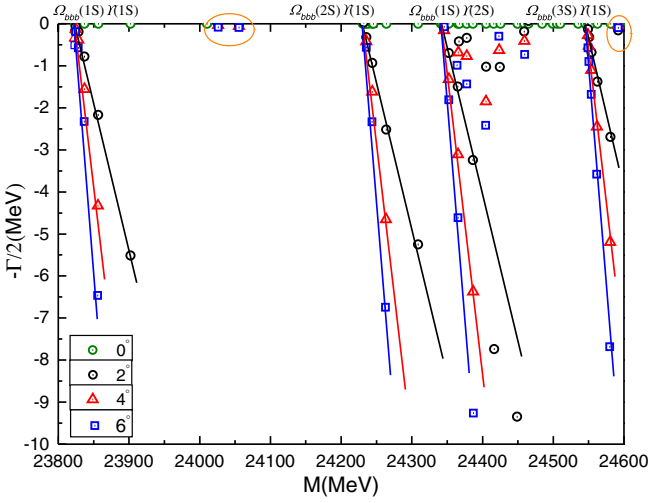

FIG. 5. Complex eigenenergies of coupled-channel calculation for various θ within $J^P = \frac{1}{2}^-$.

whose theoretical mass is 7899 MeV, remains unchanged whether coupling effects are included or not. Besides, masses of the other two exotic structures are 8421 and 8137 MeV.

Similarly to the previous J^P quantum quantum numbers, narrow resonance states are available in a fully coupled-channel investigation using the complex scaling method. Figure 4 shows our results, the scattering states of $\Omega_{ccc}(1S)J/\psi(1S)$ and its radial excitations are clearly presented within the energy range 7.9–9.0 GeV; meanwhile, three stable resonances are circled therein. Their complex energies are $(8137 + i0.18)$, $(8668 + i0.62)$, and $(8727 + i0.64)$ MeV. All of them are still compact multiquarks whose size and exotic nature are indicated in Table VIII.

B. Fully bottom pentaquarks

1. $J^P = \frac{1}{2}^-$ sector

Table IX collects the theoretical masses obtained in each fully bottom pentaquark configuration and also taking into account their couplings within the same arrangement. In particular, the color-singlet $\Omega_{bbb}\Upsilon$ configuration has a mass of 23821 MeV; the hidden-color cases of the same arrangement are located at around 24.03 GeV, except for one higher state with mass at 24.44 GeV; and when performing coupled-channel calculation, the mass is 23.96 GeV, which is above the lowest baryon-meson threshold. As for the three diquark-diquark-antiquark channels, their masses are around 24.06 GeV, and the coupling is also weak with a coupled mass generated at 24.04 GeV. At last, when a complete coupled-channel study is considered in real range approximation, the nature of the scattering state $\Omega_{bbb}\Upsilon$ is not unchanged.

Some interesting findings are obtained when a fully coupled-channel investigation has been extended to the complex range. Figure 5 shows the distribution of calculated eigenenergies within the interval 23.8–24.6 GeV. Therein, the scattering nature of $\Omega_{bbb}\Upsilon$ in both ground and radial excitation states are clearly captured. However, three fixed poles are obtained as the complex angle is rotated, and their energies read $(24026 + i0.06)$, $(24055 + i0.12)$, and $(24591 + i0.08)$ MeV. These resonances are extremely narrow, and from Table X, their sizes are close to 0.3 fm. From the same table, the first two resonances mostly consist of exotic color structures $(\sim 100\%)$, and there is a strong coupling between color-singlet (46.2%) and exotic color (53.8%) channels for the third one. Finally, the diquark-diquark-antiquark resonance with eigenenergy $(24055 + i0.12)$ MeV is compatible with the one obtained in Ref. [92].

2. $J^P = \frac{3}{2}^-$ sector

Two color-singlet baryon-meson, four hidden-color baryon-meson, and three diquark-diquark-antiquark channels are considered in this case. Table XI shows that the masses of the color-singlets $\Omega_{bbb}\eta_b$ and $\Omega_{bbb}\Upsilon$ are 23.76 and 23.82 GeV, respectively, indicating their scattering nature. Masses of the four hidden-color channels are slightly higher, lying in an energy interval from 23.94 to 24.37 GeV. Besides, the three diquark-diquark-antiquark channels are generally located at ~24.05 GeV. When computing in coupled-channels mode using real range formulation, two exotic color structures reduce their masses in about 20 MeV, and this fact does not hold for color-singlet channels. In any case, the lowest mass remains located at the $\Omega_{bbb}\eta_b$ threshold theoretical value, 23.76 GeV, even if a complete coupled-channel computation is performed.

In a fully coupled-channel investigation in which the CSM is used, two narrow resonances are obtained and shown in Fig. 6. Their complex energies read (24059 +i0.02) and (24468+i0.22) MeV. Furthermore, by analyzing their compositeness in Table XII, both compact and exotic color features are obviously shown. Finally, note that

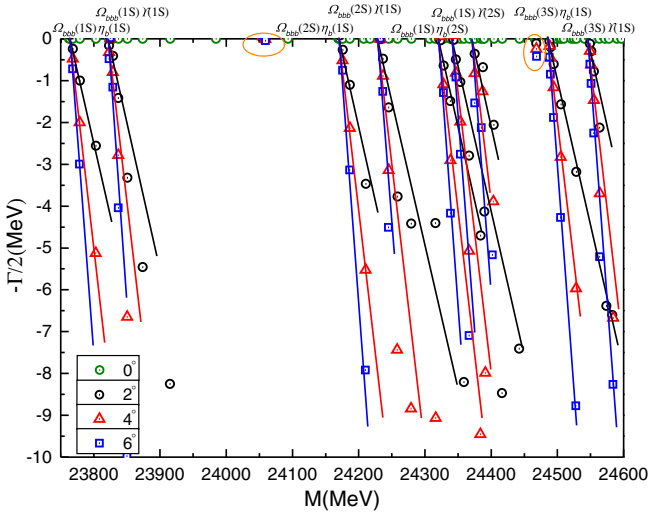

FIG. 6. Complex eigenenergies of coupled-channel calculation for various θ within $J^P = \frac{3}{2}^-$.

the 23.7–24.6 GeV energy region is plagued by discrete poles belonging to the ground and radial excitation scattering states of $\Omega_{bbb}\eta_b$ and $\Omega_{bbb}\Upsilon$.

3. $J^P = \frac{5}{2}^-$ sector

There are three channels for the highest spin sector of the fully bottom pentaquarks. Our calculated results are listed in Table XIII. First, a bound state is not possible here with the lowest mass of the color-singlet $\Omega_{bbb}\Upsilon$ channel equal to its theoretical threshold 23.82 GeV. This value remains unchanged in a fully coupled-channel case. Meanwhile, the hidden-color baryon-meson and diquark-diquark-antiquark channels are both excited, and their masses are 24.30 and 24.08 GeV, respectively.

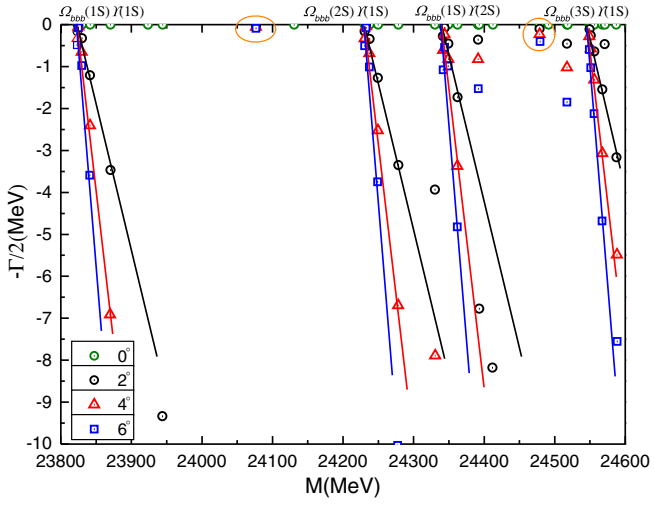

FIG. 7. Complex eigenenergies of coupled-channel calculation for various θ within $J^P = \frac{5}{2}^-$.

In a further calculation, where the CSM is employed in a complete coupled-channel study, some narrow resonances are obtained. Within the energy region 23.8–24.6 GeV of Fig. 7, two stable poles are circled among the scattering states of $\Omega_{bbb}\Upsilon$. Details on their nature are listed in Table XIV. In particular, these two resonances have masses (24076+i0.12) and (24478+i0.46) MeV, and both are compact diquark-diquark-antiquark configuration.

IV. CONCLUSIONS

The S-wave fully charm and bottom pentaquarks with spin parity $J^P = \frac{1}{2}^-$, $\frac{3}{2}^-$, and $\frac{5}{2}^-$ have been systematically investigated within both real- and complex-scaling range using a lattice-QCD inspired potential embedded in a quark model picture. The five-body Schödinger-like equation is solved by expanding the wave function solution in terms of Gaussian basis functions whose ranges are in geometric progression. Moreover, the baryon-meson and diquark-diquark-antiquark configurations, along with all of their possible color channels and coupligns, are also comprehensively considered.

Several narrow resonances are obtained in the complete coupled-channel calculations when the complex scaling range allows us to discern them. They are summarized in Table XV. All these states are exotic color configurations,

TABLE XV. Summary of the resonances found in the fully charm and bottom pentaquarks. The first column shows the spin parity of each singularity, the second column refers to the dominant channel (S: color-singlet channel, H: hidden-color channel, Di: diquark-diquark-antiquark channel), and the last column shows the corresponding complex eigenenergy, $E = M + i\Gamma$. (unit: MeV).

Fully charm pentaquarks		
J^P	Dominant channel	Complex energy
$\frac{1}{2}^-$	Di(100%)	$8098 + i0.16$
	Di(100%)	$8634 + i0.38$
	S(46%) + H(53%)	$8742 + i0.86$
$\frac{3}{2}^-$	Di(100%)	$8095 + i0.14$
	Di(100%)	$8656 + i0.62$
$\frac{5}{2}^-$	Di(100%)	$8137 + i0.18$
	Di(100%)	$8668 + i0.62$
	H(38%) + Di(51%)	$8727 + i0.64$
Fully bottom pentaquarks		
J^P	Dominant channel	Complex energy
$\frac{1}{2}^-$	H(37%) + Di(59%)	$24026 + i0.06$
	Di(100%)	$24055 + i0.12$
	S(46%) + H(52%)	$24591 + i0.08$
$\frac{3}{2}^-$	H(39%) + Di(56%)	$24059 + i0.02$
	Di(100%)	$24468 + i0.22$
$\frac{5}{2}^-$	Di(100%)	$24076 + i0.12$
	Di(100%)	$24478 + i0.46$

either hidden-color baryon-meson or diquark-diquark-antiquark structure, or by the coupling between them. The decay widths are generally small, but other possible baryon-meson decay channels with higher partial waves have not been considered, neither their three-body decay channels and potentially large electromagnetic transitions. Besides, they are usually compact arrangements of quarks whose sizes are about 0.5–0.7 and 0.2–0.4 fm for the fully charm and bottom pentaquarks, respectively. The compact feature is also indicated in several studies of heavy-flavored multiquark systems. The predicted fully heavy pentaquarks are expected to be observed in future experiments, but not without difficulties; by considering their pole positions, we propose to begin their hunting by looking at the golden decay channels $\Omega_{ccc}J/\psi$ and $\Omega_{bbb}\Upsilon$.

ACKNOWLEDGMENTS

Work was partially financed by the Zhejiang Provincial Natural Science Foundation under Grant No. LQ22A050004; National Natural Science Foundation of China under Grant Nos. 11535005 and 11775118; the Ministerio Español de Ciencia e Innovación under Grant No. PID2019–107844 GB-C22; and Junta de Andalucía, Contracts No. P18-FR-5057 and Operativo FEDER Andalucía No. 2014-2020 UHU-1264517.

[1] M. Gell-Mann, Phys. Lett. **8**, 214 (1964).
[2] G. Zweig, CERN Report No. 8182/TH.401, CERN Report No. 8419/TH.412, 1964.
[3] S. K. Choi *et al.* (Belle Collaboration), Phys. Rev. Lett. **91**, 262001 (2003).
[4] N. Brambilla *et al.*, Eur. Phys. J. C **71**, 1534 (2011).
[5] N. Brambilla *et al.*, Eur. Phys. J. C **74**, 2981 (2014).
[6] S. L. Olsen, Front. Phys. (Beijing)**10**, 121 (2015).
[7] A. Esposito, A. Pilloni, and A. D. Polosa, Phys. Rep. **668**, 1 (2017).
[8] H.-X. Chen, W. Chen, X. Liu, and S.-L. Zhu, Phys. Rep. **639**, 1 (2016).
[9] H.-X. Chen, W. Chen, X. Liu, Y.-R. Liu, and S.-L. Zhu, Rep. Prog. Phys. **80**, 076201 (2017).
[10] M. Karliner, J. L. Rosner, and T. Skwarnicki, Annu. Rev. Nucl. Part. Sci. **68**, 17 (2018).
[11] A. Ali, J. S. Lange, and S. Stone, Prog. Part. Nucl. Phys. **97**, 123 (2017).
[12] F.-K. Guo, C. Hanhart, U.-G. Meißner, Q. Wang, Q. Zhao, and B.-S. Zou, Rev. Mod. Phys. **90**, 015004 (2018).
[13] Y.-R. Liu, H.-X. Chen, W. Chen, X. Liu, and S.-L. Zhu, Prog. Part. Nucl. Phys. **107**, 237 (2019).
[14] G. Yang, J. Ping, and J. Segovia, Symmetry **12**, 1869 (2020).
[15] X.-K. Dong, F.-K. Guo, and B.-S. Zou, Phys. Rev. Lett. **126**, 152001 (2021).
[16] X.-K. Dong, F.-K. Guo, and B.-S. Zou, Commun. Theor. Phys. **73**, 125201 (2021).
[17] H.-X. Chen, Phys. Rev. D **105**, 094003 (2022).
[18] L. Meng, B. Wang, G.-J. Wang, and S.-L. Zhu (2022).
[19] R. Aaij *et al.* (LHCb Collaboration), Phys. Rev. D **102**, 112003 (2020).
[20] R. Aaij *et al.* (LHCb Collaboration), Phys. Rev. Lett. **125**, 242001 (2020).
[21] M. Ablikim *et al.* (BESIII Collaboration), arXiv:2201.10796.
[22] M. Ablikim *et al.* (BESIII Collaboration), arXiv:2112.14369.
[23] M. Ablikim *et al.* (BESIII Collaboration), Phys. Rev. Lett. **126**, 102001 (2021).
[24] R. Aaij *et al.* (LHCb Collaboration), Phys. Rev. Lett. **127**, 082001 (2021).
[25] M. Ablikim *et al.* (BESIII Collaboration), arXiv:2204.07800.
[26] R. Aaij *et al.* (LHCb Collaboration), J. High Energy Phys. 04 (2022) 046.
[27] M. Ablikim *et al.* (BESIII Collaboration), arXiv:2203.05815.
[28] R. Aaij *et al.* (LHCb Collaboration), Nat. Phys. (2022).10.1038/s41567-022-01614-y
[29] R. Aaij *et al.* (LHCb Collaboration), Nat. Commun. **13**, 3351 (2022).
[30] R. Aaij *et al.* (LHCb Collaboration), Phys. Rev. Lett. **115**, 072001 (2015).
[31] R. Aaij *et al.* (LHCb Collaboration), Phys. Rev. Lett. **122**, 222001 (2019).
[32] R. Aaij *et al.* (LHCb Collaboration), Phys. Rev. Lett. **128**, 062001 (2022).
[33] R. Aaij *et al.* (LHCb Collaboration), Sci. Bull. **66**, 1391 (2021).
[34] S. Weinberg, Phys. Rev. Lett. **110**, 261601 (2013).
[35] E. Braaten, C. Langmack, and D. H. Smith, Phys. Rev. D **90**, 014044 (2014).
[36] S. J. Brodsky and R. F. Lebed, Phys. Rev. D **91**, 114025 (2015).
[37] W. Chen, H.-X. Chen, X. Liu, T. G. Steele, and S.-L. Zhu, Phys. Lett. B **773**, 247 (2017).
[38] E. J. Eichten and C. Quigg, Phys. Rev. Lett. **119**, 202002 (2017).
[39] J.-M. Richard, A. Valcarce, and J. Vijande, Phys. Rev. C **97**, 035211 (2018).
[40] P. G. Ortega, J. Segovia, D. R. Entem, and F. Fernández, Eur. Phys. J. C **79**, 78 (2019).
[41] M. A. Bedolla, J. Ferretti, C. D. Roberts, and E. Santopinto, Eur. Phys. J. C **80**, 1004 (2020).
[42] P. G. Ortega, J. Segovia, and F. Fernandez, Phys. Rev. D **104**, 094004 (2021).

[43] A. Esposito, C. A. Manzari, A. Pilloni, and A. D. Polosa, Phys. Rev. D **104**, 114029 (2021).
[44] G. Balassa and G. Wolf, Eur. Phys. J. A **57**, 246 (2021).
[45] C. Cheng, F. Yang, and Y. Huang, Phys. Rev. D **104**, 116007 (2021).
[46] M.-L. Du, Z.-H. Guo, and J. A. Oller, Phys. Rev. D **104**, 114034 (2021).
[47] N. Yalikun, Y.-H. Lin, F.-K. Guo, Y. Kamiya, and B.-S. Zou, Phys. Rev. D **104**, 094039 (2021).
[48] J.-Z. Wang, X. Liu, and T. Matsuki, Phys. Rev. D **104**, 114020 (2021).
[49] C.-h. Chen, Y.-L. Xie, H.-g. Xu, Z. Zhang, D.-M. Zhou, Z.-L. She, and G. Chen, arXiv:2111.03241.
[50] M.-L. Du, EPJ Web Conf. **258**, 04007 (2022).
[51] J.-M. Xie, X.-Z. Ling, M.-Z. Liu, and L.-S. Geng, arXiv:2204.12356.
[52] Z.-L. Wang, C.-W. Shen, D. Rönchen, U.-G. Meißner, and B.-S. Zou, Eur. Phys. J. C **82**, 497 (2022).
[53] C.-R. Deng, arXiv:2202.13570.
[54] I. W. Park, S. H. Lee, S. Cho, and Y. Kim, Phys. Rev. D **105**, 114023 (2022).
[55] R. Chen and X. Liu, Phys. Rev. D **105**, 014029 (2022).
[56] T. J. Burns and E. S. Swanson, Eur. Phys. J. A **58**, 68 (2022).
[57] F. Yang, Y. Huang, and H. Q. Zhu, Sci. China Phys. Mech. Astron. **64**, 121011 (2021).
[58] P.-P. Shi, F. Huang, and W.-L. Wang, Eur. Phys. J. A **57**, 237 (2021).
[59] M.-W. Li, Z.-W. Liu, Z.-F. Sun, and R. Chen, Phys. Rev. D **104**, 054016 (2021).
[60] X.-Z. Ling, J.-X. Lu, M.-Z. Liu, and L.-S. Geng, Phys. Rev. D **104**, 074022 (2021).
[61] T.-W. Wu, Y.-W. Pan, M.-Z. Liu, J.-X. Lu, L.-S. Geng, and X.-H. Liu, Phys. Rev. D **104**, 094032 (2021).
[62] W. Ruangyoo, K. Phumphan, C.-C. Chen, A. Limphirat, and Y. Yan, J. Phys. G **49**, 075001 (2022).
[63] P. Ling, X.-H. Dai, M.-L. Du, and Q. Wang, Eur. Phys. J. C **81**, 819 (2021).
[64] J.-X. Lu, M.-Z. Liu, R.-X. Shi, and L.-S. Geng, Phys. Rev. D **104**, 034022 (2021).
[65] Q. Wu, D.-Y. Chen, and R. Ji, Chin. Phys. Lett. **38**, 071301 (2021).
[66] M.-L. Du, V. Baru, F.-K. Guo, C. Hanhart, U.-G. Meißner, J. A. Oller, and Q. Wang, J. High Energy Phys. 08 (2021) 157.
[67] C. W. Xiao, J. J. Wu, and B. S. Zou, Phys. Rev. D **103**, 054016 (2021).
[68] J.-T. Zhu, L.-Q. Song, and J. He, Phys. Rev. D **103**, 074007 (2021).
[69] R. Chen, Eur. Phys. J. C **81**, 122 (2021).
[70] M.-J. Yan, F.-Z. Peng, M. S. Sánchez, and M. P. Valderrama, arXiv:2108.05306.
[71] G. Yang, J. Ping, and F. Wang, Phys. Rev. D **95**, 014010 (2017).
[72] P. Yang and W. Chen, arXiv:2203.15616.
[73] Y. Huang and H. Q. Zhu, Phys. Rev. D **104**, 056027 (2021).
[74] J.-T. Zhu, S.-Y. Kong, Y. Liu, and J. He, Eur. Phys. J. C **80**, 1016 (2020).
[75] G. Yang, J. Ping, and J. Segovia, Phys. Rev. D **99**, 014035 (2019).
[76] Q. Zhang, X.-H. Hu, B.-R. He, and J.-L. Ping, Eur. Phys. J. C **81**, 224 (2021).
[77] Y. Xing, W.-L. Liu, and Y.-H. Xiao, arXiv:2203.03248.
[78] U. Özdem, arXiv:2201.00979.
[79] Y. Xing and Y. Niu, Eur. Phys. J. C **81**, 978 (2021).
[80] R. Chen, N. Li, Z.-F. Sun, X. Liu, and S.-L. Zhu, Phys. Lett. B **822**, 136693 (2021).
[81] K. Chen, B. Wang, and S.-L. Zhu, Phys. Rev. D **103**, 116017 (2021).
[82] G. Yang, J. L. Ping, and J. Segovia, Phys. Rev. D **101**, 074030 (2020).
[83] V. Khachatryan *et al.* (CMS Collaboration), J. High Energy Phys. 05 (2017) 013.
[84] K. Yi, Int. J. Mod. Phys. A **33**, 1850224 (2018).
[85] L. C. Bland *et al.* (ANDY Collaboration), arXiv:1909.03124.
[86] R. Aaij *et al.* (LHCb Collaboration), J. High Energy Phys. 10 (2018) 086.
[87] A. M. Sirunyan *et al.* (CMS Collaboration), Phys. Lett. B **808**, 135578 (2020).
[88] R. Aaij *et al.* (LHCb Collaboration), Sci. Bull. **65**, 1983 (2020).
[89] Y. Yan, Y. Wu, X. Hu, H. Huang, and J. Ping, Phys. Rev. D **105**, 014027 (2022).
[90] H.-T. An, K. Chen, Z.-W. Liu, and X. Liu, Phys. Rev. D **103**, 074006 (2021).
[91] H.-T. An, S.-Q. Luo, Z.-W. Liu, and X. Liu, Phys. Rev. D **105**, 074032 (2022).
[92] Z.-G. Wang, Nucl. Phys. **B973**, 115579 (2021).
[93] J.-R. Zhang, Phys. Rev. D **103**, 074016 (2021).
[94] T. Kawanai and S. Sasaki, Phys. Rev. D **85**, 091503 (2012).
[95] G. Yang, J. Ping, and J. Segovia, Phys. Rev. D **104**, 014006 (2021).
[96] E. Hiyama, Y. Kino, and M. Kamimura, Prog. Part. Nucl. Phys. **51**, 223 (2003).
[97] J. Aguilar and J. M. Combes, Commun. Math. Phys. **22**, 269 (1971).
[98] E. Balslev and J. M. Combes, Commun. Math. Phys. **22**, 280 (1971).
[99] B. Simon, Commun. Math. Phys. **27**, 1 (1972).
[100] Y. Ho, Phys. Rep. **99**, 1 (1983).
[101] E. Eichten, K. Gottfried, T. Kinoshita, J. B. Kogut, K. D. Lane, and T.-M. Yan, Phys. Rev. Lett. **34**, 369 (1975); **36**, 1276(E) (1976).
[102] E. Eichten, K. Gottfried, T. Kinoshita, K. D. Lane, and T.-M. Yan, Phys. Rev. D **21**, 203 (1980).
[103] J. Zhao, K. Zhou, S. Chen, and P. Zhuang, Prog. Part. Nucl. Phys. **114**, 103801 (2020).
[104] G. Yang, J. Ping, P. G. Ortega, and J. Segovia, Chin. Phys. C **44**, 023102 (2020).
[105] G. Yang and J. Ping, Phys. Rev. D **97**, 034023 (2018).
[106] G. Yang, J. Ping, and J. Segovia, Phys. Rev. D **102**, 054023 (2020).
[107] G. Yang, J. L. Ping, and J. Segovia, Phys. Rev. D **101**, 014001 (2020).